

Branching Copy-Number Evolution and Parallel Immune Profiles across the Regional Tumor Space of Resected Pancreatic Cancer



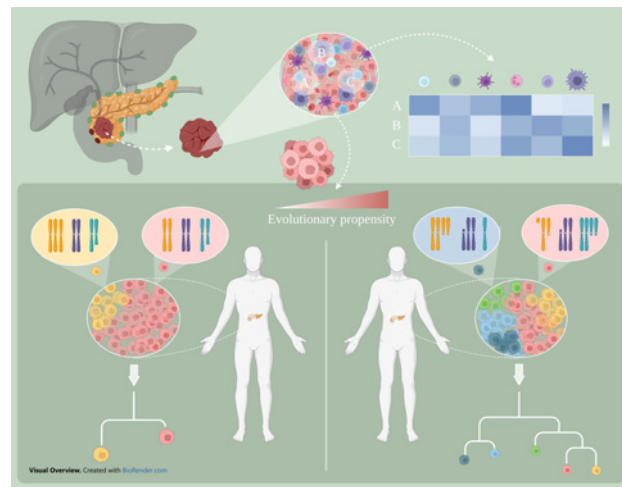
Alexandra Petersson¹, Natalie Andersson², Sofie Olsson Hau¹, Jakob Eberhard¹, Jenny Karlsson², Subhayan Chattopadhyay², Anders Valind^{2,3}, Jacob Elebro¹, Björn Nodin¹, Karin Leandersson⁴, David Gisselsson^{1,2}, and Karin Jirström¹

ABSTRACT

Pancreatic ductal adenocarcinoma (PDAC) remains a highly lethal disease. The only option for curative treatment is resection of the tumor followed by standard adjuvant chemotherapy. Yet, early relapse due to chemoresistance is almost inevitable. Herein, we delineated the genetic intratumor heterogeneity in resected PDAC, with the aim to identify evolutionary patterns that may be associated with overall survival (OS) following treatment with curative intent. Potential relationships with the adjacent immune microenvironment were also examined. The genetic and immune landscapes of the regional tumor space were analyzed in nine patients with resected PDAC. Targeted deep sequencing and genome wide SNP array were followed by clonal deconvolution and phylogenetic analysis. A mathematical complexity score was developed to calculate the network extent of each phylogeny. Spatial variation in abundance and tumor nest infiltration of immune cells was analyzed by double IHC staining. Copy-number heterogeneity was denoted as the major contributing factor to the branching architectures of the produced phylogenetic trees. Increased tree complexity was significantly inversely associated with OS, and larger regional maximum aberrations (higher treetops) were associated with increased PD-L1 expression on tumor cells. Contrastingly, an *FREMI* gene amplification, found in one patient, coincided with a particularly vigorous immune response. Findings from this limited case series suggest that complex evolutionary patterns may be associated

with a shorter survival in surgically treated patients with PDAC. Some hypothesis-generating associations with the surrounding immune microenvironment were also detected.

Implications: Evolutionary copy-number patterns may be associated with survival in patients with resected PDAC.



Introduction

In the wake of an expanding therapeutic arsenal, treatment resistance has become a considerable challenge to the clinical management of patients with cancer. The evolutionary nature of tumors, driven by Darwinian natural selection, constantly promotes clones with higher fitness and, thus, accounts for a significant degree of therapeutic resilience (1, 2). Intratumor heterogeneity (ITH), the presence of various subclonal populations within a tumor, provides a perfect substrate on which selection pressures from systemic therapies may act (3). The prognosis for patients diagnosed with pancreatic ductal adenocarcinoma (PDAC), one of the leading causes of cancer-related death (4–6), underlines the consequence of treatment resistance. Almost concurrent incidence and mortality rates are seen as a result of late diagnosis, limited treatment options, and a profound lack of complementary biomarkers (7, 8). The only curative treatment is resection of the tumor followed by standard adjuvant chemotherapy, but less than 20% of the patients are eligible for surgery (9), and in the majority of cases, the disease will recur within a year due to chemoresistance (10).

¹Division of Oncology and Therapeutic Pathology, Department of Clinical Sciences Lund, Lund University, Lund, Sweden. ²Division of Clinical Genetics, Department of Laboratory Medicine, Lund University, Lund, Sweden. ³Department of Pediatrics, Skåne University Hospital, Lund, Sweden. ⁴Cancer Immunology, Department of Translational Medicine, Lund University, Malmö, Sweden.

Note: Supplementary data for this article are available at Molecular Cancer Research Online (<http://mcr.aacrjournals.org/>).

Corresponding Author: Alexandra Petersson, Lund University, Barngatan 4, Lund, Skåne, 22185 Sweden. Phone: 467-0572-5302; E-mail: alexandra.petersson@med.lu.se

Mol Cancer Res 2022;20:749–61

doi: 10.1158/1541-7786.MCR-21-0986

This open access article is distributed under Creative Commons Attribution-NonCommercial-NoDerivatives License 4.0 International (CC BY-NC-ND).

©2022 The Authors; Published by the American Association for Cancer Research

Major efforts have been made in the genomic characterization of PDAC, revealing a complex picture with extensive interpatient heterogeneity (11–14). Numerous mutations and copy-number variations (CNV) have been identified that affect genes of importance to pancreatic tumorigenesis, frequently including *KRAS*, *TP53*, *CDKN2A*, and *SMAD4*. These alterations are further accompanied by a shifting mutational landscape of less frequent variants (15), and recent studies focusing on deciphering the ITH and clonal evolution of advanced PDAC have shown that mutations of less known significance account for the greater part of the detected genetic diversity (16–18). Accordingly, a deeper understanding of the drivers of subclonal evolution and adaptation in PDAC is needed. In particular, somatic CNVs, that is, regional genome gains or losses, are known to be important for tumor progression (19), but in comparison with single nucleotide variants (SNV), their evolutionary role has been understudied. In addition, recent work has mainly focused on depicting the evolutionary trajectories in advanced metastatic disease (16–19), leaving an unmet need to explore the clonal geography across the regional tumor area in treatment naïve primary PDAC. Ideally, such a characterization should include an account of how tumor cell diversity allows for selection of clones able to resist, control, and exploit the microenvironment. A dynamic interplay between clonal evolution and infiltrating immune cells (IC) has recently been described in lung cancer, wherein tumor regions are pushed by the ICs to develop defense mechanisms enabling immune evasion (20). The microenvironment of PDAC has traditionally been described as immunosuppressive (21), although the combination of certain immune signatures and genomic tumor characteristics has been shown to carry prognostic and predictive significance (22). Still, the extent to which the surrounding immune response shapes the regional clonal evolution in treatment naïve PDAC remains to be characterized.

Herein, we performed an extensive mapping of genomic ITH, by whole-genome copy-number analysis and targeted deep sequencing (TDS), and inferred phylogenetic relationships between detected genetic clones in resected primary tumors and regional lymph node metastases from nine patients with PDAC. The aim was to identify evolutionary patterns that may be associated with overall survival (OS) following treatment with curative intent. The in-depth genomic characterization was also accompanied by spatial analysis of the surrounding immune microenvironment to explore any potential associations between the two.

Materials and Methods

Study cohort

The cases in this study are derived from a retrospective consecutive cohort of 39 patients diagnosed with primary PDAC who underwent pancreaticoduodenectomy at Skåne University Hospital, Lund, between January 1, 2012 and December 31, 2014. Acquisition of histopathological and clinical data is further described in Supplementary File S1, Supplementary Methods. The study was conducted with approval from the Ethics committee of Lund University (reference number 445/07, 2008/35, 2011/670 and 2014/748), whereby approval was given for an opt-out consent. This project has been carried out in accordance with European and national requirements; decision no. 1110/94/EC of the European Parliament and of the Council (OJL126 18,5,94) and the Declaration of Helsinki on ethical principles for medical research involving human subjects.

Spatial analysis of the immune microenvironment

To evaluate the spatial heterogeneity of the immune microenvironment, individual tissue microarrays for each patient, “Single Patient Tissue Chips” (SPTC) were constructed as previously described (23). A summary of the SPTC construction and a detailed description of the subsequent IHC analysis are available in Supplementary File S1. In brief, a combination of two immune markers (nine markers in total) was used in each staining procedure to enable IC subset detection in terms of both abundance and tumor nest (TN) infiltration.

Spatial genetic profiling

To explore spatial genetic heterogeneity, a third tissue core was obtained from each tumor-enriched area selected for SPTC construction and used for genomic analyses. In total, 93 formalin-fixed paraffin-embedded (FFPE) samples (72 from primary tumors and 21 from regional lymph node metastases) were subjected to whole-genome copy-number analysis using the SNP array OncoScan CNV assay (Affymetrix) according to standard protocols. All tumor samples found to contain allelic imbalances (72/93 analyzed), along with paired normal samples and two additional regional lymph node samples, were selected for TDS using the extensive INVIEW Oncopanel All-in-one (version 2.7; Eurofins Genomics). The selected panel covers the entire exons of more than 590 cancer-associated genes (Supplementary File S2) and is optimized for FFPE samples. A flowchart of all sampled tumor areas selected for genomic profiling, along with the analysis pipeline, is presented in Supplementary File S3 and a detailed description of all subsequent data analysis is available in Supplementary File S1.

Clonal deconvolution and phylogenetic analysis based on chromosomal alterations and mutations with known deleterious effects

Clone size calculations were performed on the basis of both relative probe intensity ratios ($\log_2 R$ value) for each CNV and variant allele frequencies for each TDS-detected variant, SNVs and insertions and deletions (InDels), by use of previously well-established methods (refs. 24–27; details in Supplementary File S1). To further deduce the most likely evolutionary trajectory resulting from each tumor's unique genetic clonal landscape, all detected CNVs along with known deleterious SNVs and InDels, were analyzed using the DEVOLUTION algorithm (28), described in Supplementary File S1. In total, subsequent to exclusion of samples with scarce tumor cell fraction (TCF), 40 samples (35 primary tumor, 5 lymph node metastasis) originating from nine patients were eligible for evolutionary reconstruction as a phylogeny of clones (Supplementary File S4, Supplementary Table S1) based on all detected genetic alterations and corresponding clone size estimations (Supplementary File S4, Supplementary Table S2).

Complexity score

To delineate the evolutionary complexity of each tumor's phylogeny, complementary to other more elementary phylogenetic tree attributes, we developed a complexity score (method details in Supplementary File S1) to summarize the network extent of each tree into a single value, based on previously derived formulas on decision trees (29). In brief, all produced copy number–based phylogenies were translated into a decision tree format, assigning each branching point and detected subclone to a specific generation, increasing in value with nested subclonality. In addition, the formula was designed to be scalable to the number of connections, that is, genetic drift

(Supplementary File S5, Supplementary Figs. S1–S3). Following decision tree translations, calculations of the total tree complexity score were performed for each phylogeny, dependent on both the branching architecture and the number of detected clones (Supplementary File S5, Supplementary Figs. S4–S5).

Clonal deconvolution and phylogenetic analysis based on SNVs only

All SNVs detected by TDS, regardless of previously known pathogenic effects, were subjected to an additional clonal deconvolution and evolutionary analysis using DEVOLUTION (detailed bioinformatic pipeline in Supplementary File S1; ref. 28). In summary, 34 samples (30 primary tumor, 4 lymph node metastases) originating from eight patients were eligible for SNV-based evolutionary analysis, founded by all SNVs and corresponding clone size estimations (Supplementary File S4, Supplementary Table S3).

Statistical analysis

Linear regression analysis was performed to evaluate associations between different genetic parameters, tree characteristics, patient OS and tumor infiltrating ICs, by using the *lm* function in the R package *stats*, or the *stat_cor* function in the R package *ggpubr* together with the *geom_smooth* function (method = *lm*) in the R package *ggplot2* (30). Multivariable regression analysis was performed to determine the association between complexity score and OS, accounting for vascular invasion, by the *lm* function in the R package *stats*. Moreover, the Pearson χ^2 test with Yate's continuity correction was used to explore the prognostic value of specific chromosomal aberrations, with Bonferroni correction for multiple testing. Throughout the study, a *P* value of <0.05 was considered as significant. All statistical analyses were conducted in R (version 3.6.0; ref. 31) and RStudio (version 1.2.1335).

Availability of data and materials

Complete curated data from the SNP array analysis may be found in Supplementary File S4, Supplementary Table S4, and from the TDS analysis for mutations with known deleterious effects in Supplementary File S4, Supplementary Table S5. All raw datasets used and/or analyzed during the current study will be made available from the corresponding author upon request in compliance with Swedish legislation.

Results

Clinicopathological and genetic characteristics

Clinicopathological characteristics of the nine primary patients with PDAC included in the study are summarized in Supplementary File S4, Supplementary Table S6. From each patient, multiple tissue samples were obtained from the primary tumor area, including regional nodal metastases when present, and analyzed by genome-wide SNP array analysis and TDS (Supplementary File S4, Supplementary Tables S2, S4, and S5). The median number of samples per patient was 5 (range, 3–6; Fig. 1). The genomic copy-number profile of each tumor is visualized in Fig. 2, and in Supplementary File S6, Supplementary Fig. S1, normalized to the estimated ploidy state of each sample, with the median number of detected alterations for all samples being 25.5 (range, 10–72). Allelic loss of *TP53* and *SMAD4* was observed in all nine cases. By sequencing, we identified point mutations and small insertions/deletions in known drivers of PDAC such as *KRAS* (9/9), *TP53* (8/9), *SMAD4* (5/9), and *CDKN2A* (2/9; Fig. 3A; refs. 12, 17). Homozygous copy-number deletions of *CDKN2A* were also found by SNP array analysis in patients 3, 5, and 8. Additional candidate driver

alterations found were a loss-of-function variant in Ring Finger Protein 43 (*RNF43*^{p.R145}) in patient 1, a gain-of-function mutation in the oncogene encoding the stimulatory G-protein α_s (*GNAS*^{p.R201C}) in patient 4, and a missense loss-of-function variant in the Dihydropyrimidine dehydrogenase (*DPYD*^{p.E423K}) gene in one sample originating from patient 3 (Supplementary File S4, Supplementary Table S5). The functional status of the altered tumor-suppressor genes detected in this study and information about the zygosity at each locus is shown in Fig. 3B. Focal gene amplifications were scarce throughout the material, but to name a few, amplification of the *MYC* oncogene was detected in patient 4 and an amplification of chromosome band 9p22 was found in patient 9, harboring the Cerberus 1 (*CER1*) and FRAS1-related extracellular matrix 1 (*FREMI1*) genes.

Branching copy-number evolution

Intratumor genetic heterogeneity was prominent in most cases and included complex patterns of CNVs as exemplified by patient 5 (Fig. 2) where chromosome 4 displayed three different allelic compositions: 1+1, 1+0, and 2+0. For patients 3, 7, and 9, there was evidence of an early whole-genome doubling event as the majority of the chromosomes were either tetrasomic (patient 3 and 9), or trisomic (patient 7). To systematically study intratumor diversity, clonal deconvolution and temporal analysis was performed to identify evolutionary relationships and spatial heterogeneity, that is, differences in genomic profiles, throughout the tumor space. Intratumor copy-number heterogeneity was detected to various degrees in all patients, whereas heterogeneity of variants in known driver genes was only found in patients 3, 5, and 8 (Fig. 4; Supplementary File S6, Supplementary Figs. S2–S4), with patient 8 showing evidence of parallel evolution with two independent *SMAD4* variants (*p.R361H* and *p.R34*). The limited detected heterogeneity of point mutations was also evident when performing a second phylogenetic analysis (8/9 patients) based on SNVs only, regardless of previously known deleterious effects (Supplementary File S6, Supplementary Fig. S5). However, although some of the SNV tree branching structures resembled the CNV-based phylogenies (e.g., patients 5 and 8), copy-number heterogeneity was denoted as the major contributing factor to the branching architectures of the phylogenetic trees.

Through detailed examination of the copy-number data, we further distinguished varying branching patterns, with both early (e.g., patient 5) and late (e.g., patient 7) segregation from the tree trunk (Supplementary File S6, Supplementary Figs. S2–S4), along with different subclonal nesting features. A mixture of linear and collateral evolution was evident in all patients, except for patient 1, where only the latter was notable. In four patients, we also obtained genetic information from lymph node metastases (patients 2, 4, 6, and 8), and were able to deduce the point where the metastatic clones branched out from the other lineages. This branching point appeared to be an early evolutionary event in most cases (patients 2, 4, and 8), as the metastatic clones in these patients only share stem alterations with the primary tumor. With regard to patient 6, however, the lymph node metastasis appeared to originate from a subclone present in sample P1. To validate that these early dissemination patterns were not biased by a low TCF in the lymph node metastasis samples, we assessed the correlation between the number of detected CNVs and the respective TCF value in each individual sample. As shown in Supplementary File S7, Supplementary Fig. S1, no significant correlation was evident.

A detailed analysis was further performed to evaluate the evolutionary value of specific CNV acquisitions and different CNV subclasses. The presence of known prevalent structural variations in

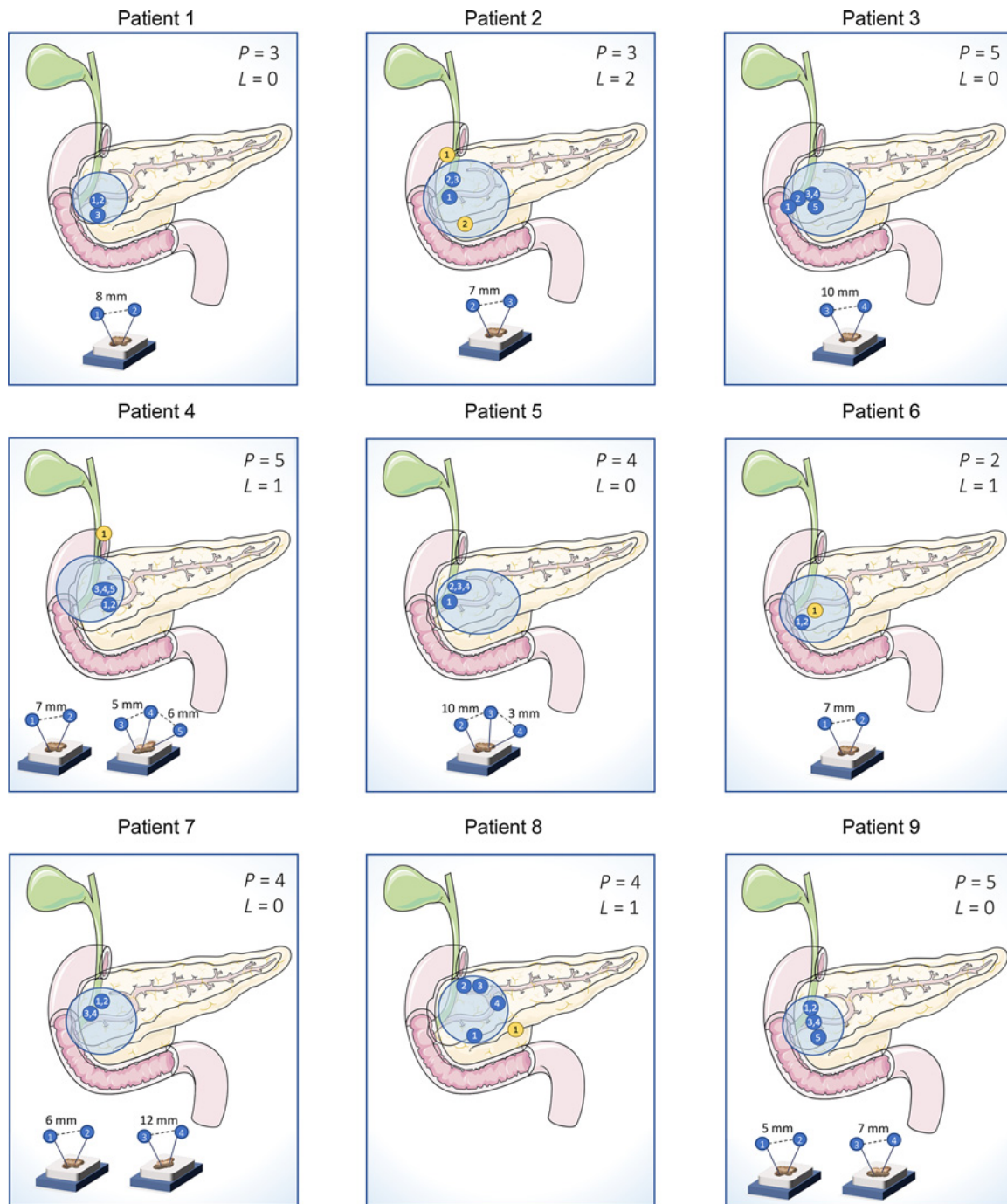


Figure 1.

An overview of areas within the regional tumor space, for the nine PDAC patients, from where samples included in the phylogenetic analyses were obtained. All patients underwent pancreaticoduodenectomy and the approximate size and location for each tumor is visualized by the larger blue transparent circle. The smaller circles show the anatomic site of the different FFPE blocks included, where blue indicates primary tumor and yellow indicates lymph node metastases. The distance between samples originating from the same FFPE block was measured and is shown where applicable. *P*, number of primary samples; *L*, number of lymph node metastases. This figure was created using templates from Servier Medical Art, licensed under a Creative Commons Attribution 3.0 Unported license; <https://creativecommons.org/licenses/by/3.0/>.

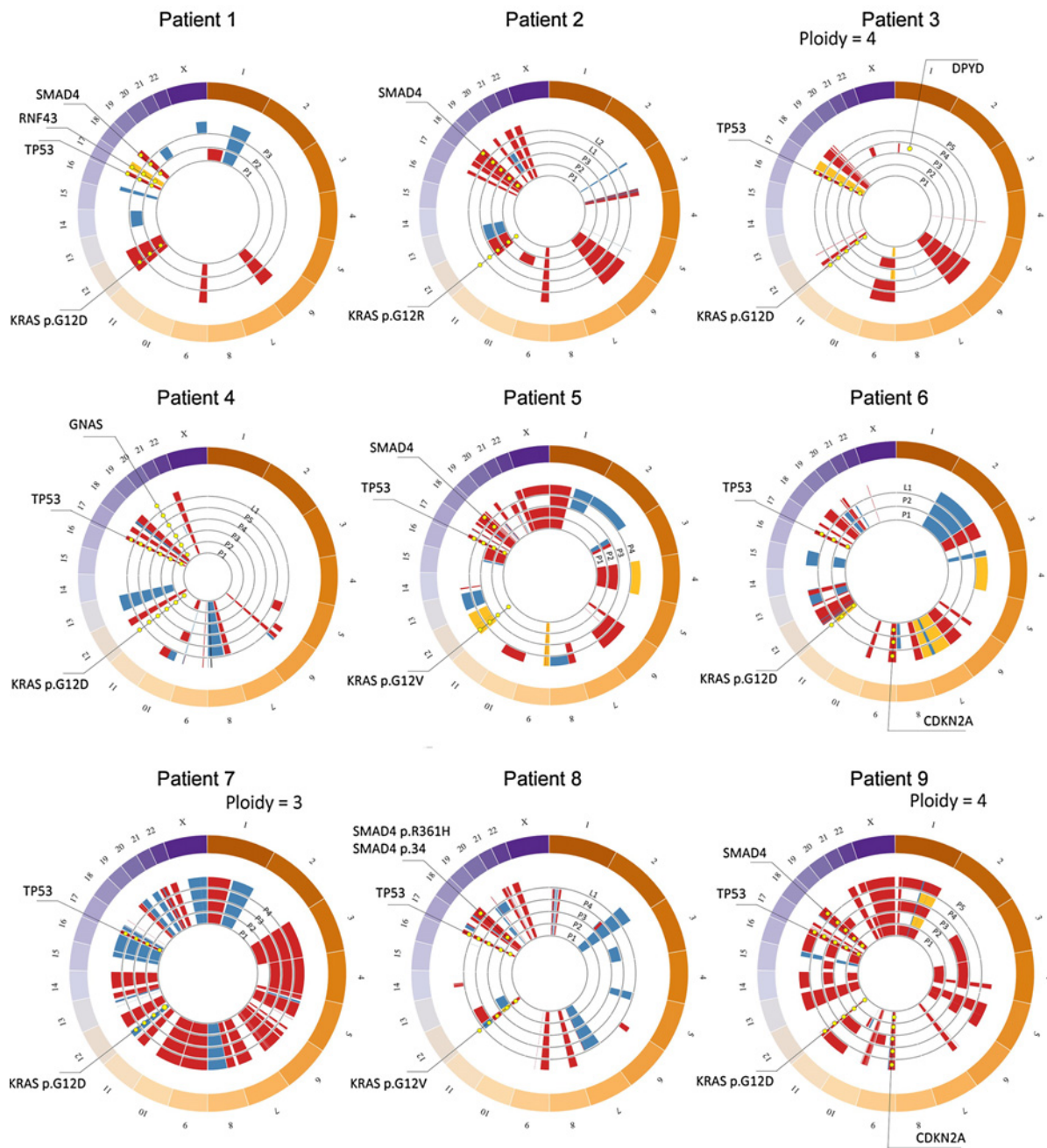


Figure 2.

Copy-number profiles for each PDAC tumor. Circos plots visualizing CNVs detected within each chromosome for all nine patients, each inner circle corresponding to the various samples included. Copy-number losses are shown in red, gains in blue, CNIs in yellow, and amplifications in black. Estimated ploidy state of tumors showing evidence of aneuploidy is noted where applicable, and all copy-number profiles have further been normalized to the estimated ploidy state of each sample before visualization. Genes affected by known deleterious mutations are annotated for each individual sample.

PDAC, according to a previous large study (32), was explored in all tumors in relation to OS (Supplementary File S6, Supplementary Fig. S6). Heterozygous loss of the p-arm of chromosome 8 was the sole aberration significantly associated to patient survival ($P < 0.05$) but was not significant when correcting for multiple testing. Nevertheless, the exclusive loss of $8p$ in patients with a shorter survival was also notable in the combined whole-genome view for all samples (Supple-

mentary File S6, Supplementary Fig. S7). In addition, the median number of each CNV class (i.e., gain, loss and copy-number neutral imbalance = CNI) was calculated for each patient and correlated to OS using univariate linear regression (Supplementary File 6, Supplementary Fig. S8). A significant association was observed for an increased number of gains and a shorter OS, but this significance was lost following correction for multiple tests.

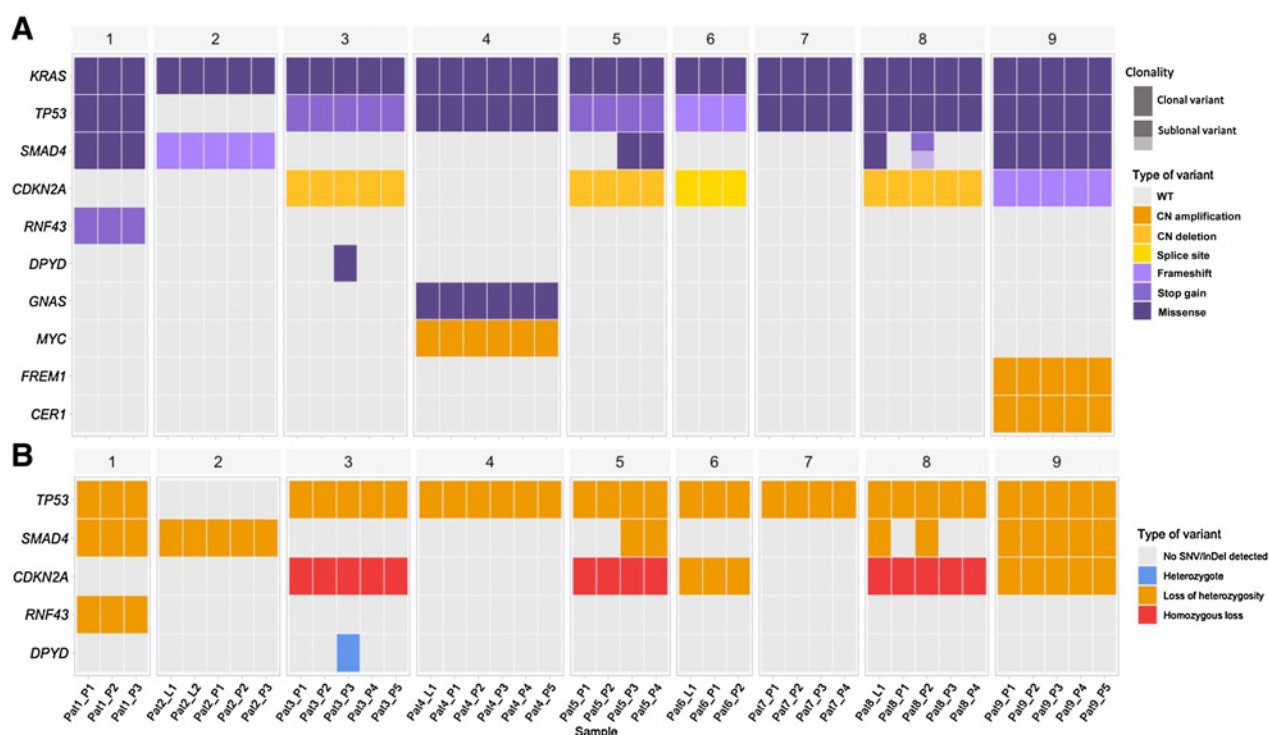


Figure 3. Genes altered by known deleterious mutations and copy-number alterations in each PDAC tumor. **A**, A summary of genes altered by mutations of known clinical relevance or affected by homozygous copy-number deletions or amplifications in each tumor sample. Variants are color coded according to the type of genetic change responsible; missense, frameshift, stop gain, splice site, homozygous copy-number (CN) deletion or amplification. Each variant is also annotated according to its estimated clonality status in each sample, clonal or subclonal. **B**, Allelic CN status for the genomic regions covering tumor-suppressor genes, with a detected SNV/Indel, and genes affected by a homozygous copy-number loss, for each patient. LOH, Loss of heterozygosity; HO loss, homozygous loss; Heterozygote, no detected change in CN status.

Tree complexity is associated with survival

To be able to compare phylogenetic features beyond elementary tree characteristics, a network-based complexity score was calculated for each tree, taking the branching architecture into account as well as the number of subclones (Fig. 5A; Supplementary File S5, Supplementary Figs. S4–S5). The complexity score was compared with patient survival time after surgery by univariate linear regression analysis (Fig. 5B). An increase in network complexity was significantly ($P < 0.001$) associated with a shorter survival time. The associations between OS and other tree characteristics are summarized in Supplementary File S7, Supplementary Fig. S2. The number of subclones detected in each tumor was the only other factor significantly associated with OS ($P = 0.02$). Because the complexity formula takes the total number of subclones into account and returned a greater explained variance (adjusted multiple R^2 : 0.81 vs. 0.50 in univariate analyses), we chose to continue with the complexity score alone in further analyses.

Effects of possible confounders, such as sampling bias and clinical differences between patients, were evaluated with univariate linear regression to confirm the detected association between tree complexity and OS (see Supplementary File S7, Supplementary Fig. S3, for parameters discussed below). As genetic information from lymph node metastases was only extractable in some of the patients, the analysis comparing tree complexity with patient outcome was also performed with primary tumor samples only. This confirmed a significant association between complexity and survival time. Fur-

thermore, no association was found between complexity scores and the total number of samples included in the phylogenies, the number of FFPE blocks from which the samples originated or tumor size. Moreover, no association was detected when comparing distances between samples obtained from the same paraffin block (see Fig. 1) and the number of non-shared alterations between them. An additional test was also carried out investigating whether the difference in TCF was responsible for the varying complexity, but no association was found.

Among the established prognostic factors (Supplementary File S4, Supplementary Table S6), only growth of the tumors into blood vessels ($P = 0.043$) and lymphatic vessels ($P = 0.015$) were found to be prognostic in univariate linear regression analyses. When including a combined vascular invasion variable; 0, no invasion; 1, growth in blood or lymphatic vessels; and 2, growth in blood and lymphatic vessels, in a multivariable regression together with the tree complexity score, the two variables increased the explained variance (adjusted multiple $R^2 = 0.93$; $P < 0.001$) with both explanatory variables carrying significance (tree complexity: $P = 0.037$, vascular invasion: $P = 0.013$).

Spatial heterogeneity of the immune microenvironment

Double IHC staining was applied to assess the abundance as well as TN infiltration of the following IC subsets (Fig. 6A); $CD3^+CD8^-$ T cells (referred to as T_H cells), $CD3^+CD8^+$ T cells (referred to as T_C cells), $FoxP3^+CD8^-$ T cells (referred to as $CD8^- T_{regs}$), $FoxP3^+CD8^+$ T cells (referred to as $CD8^+ T_{regs}$), $CD68^+CD163^-$ macrophages

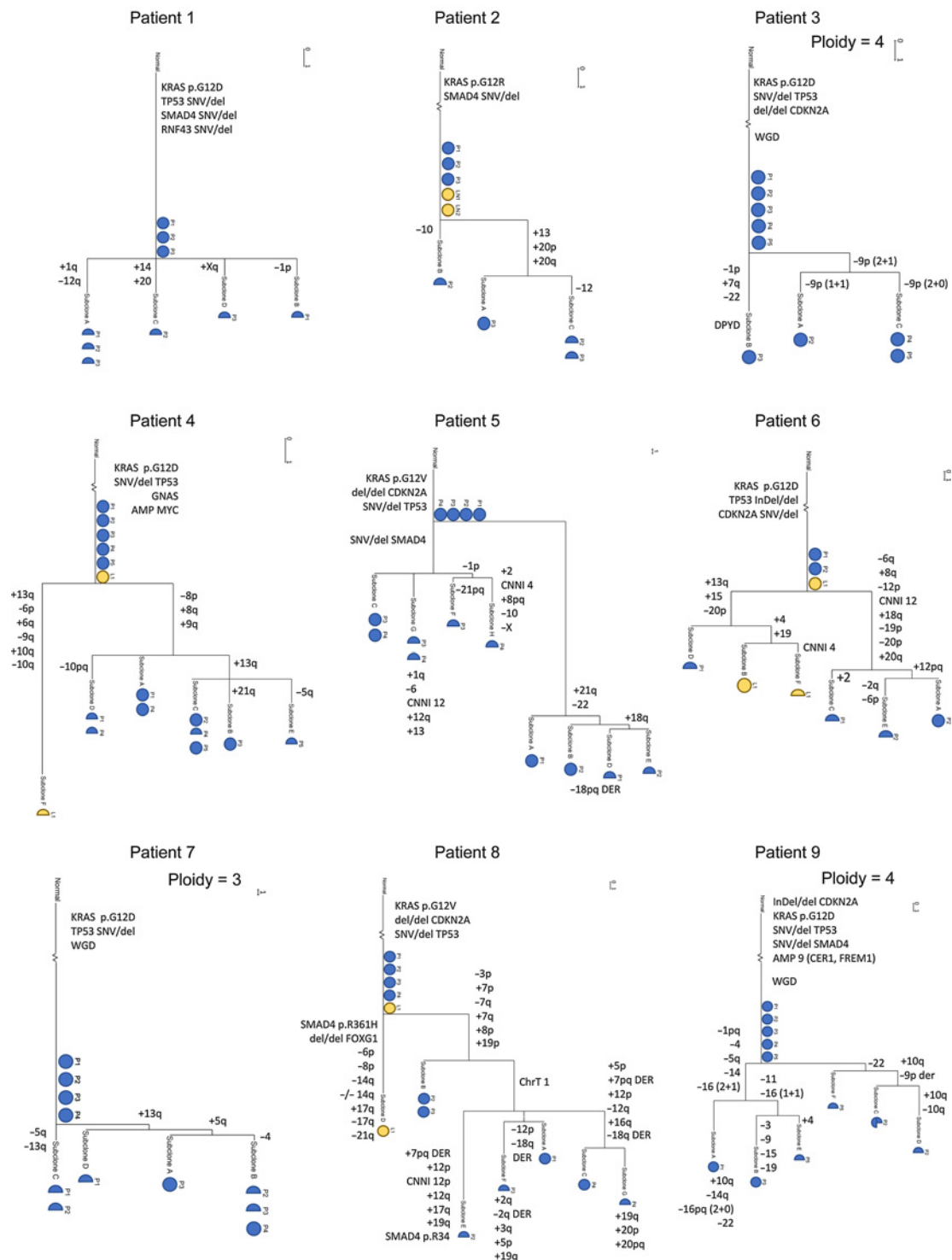


Figure 4. Phylogenetic analysis based on chromosomal alterations and mutational variants with known deleterious effects. Phylogenies illustrating the ancestral relationship between genetic clones detected in each sample, by using the maximum likelihood (ML) algorithm, for all tumors, rooted in a normal cell. A scale, indicating the corresponding length of one aberration, is shown in the top right of each tree. Each vertical branch is annotated with the associated detected CNVs, SNVs, and InDels, except in the stem where only altered genes and whole-genome doubling (WGD) events are shown. For mutations in tumor-suppressor genes, double hits are further noted, where del = copy-number deletion. A complete circle indicates that the alterations of that particular subclone were present in all tumor cells in the noted sample (clonal), whereas a semicircle marks that only a part of the cells in that sample harbored the alterations (subclonal). Blue and yellow circles correspond to primary tumor samples, and lymph node metastases, respectively. Tumors were estimated as being diploid if not stated otherwise.

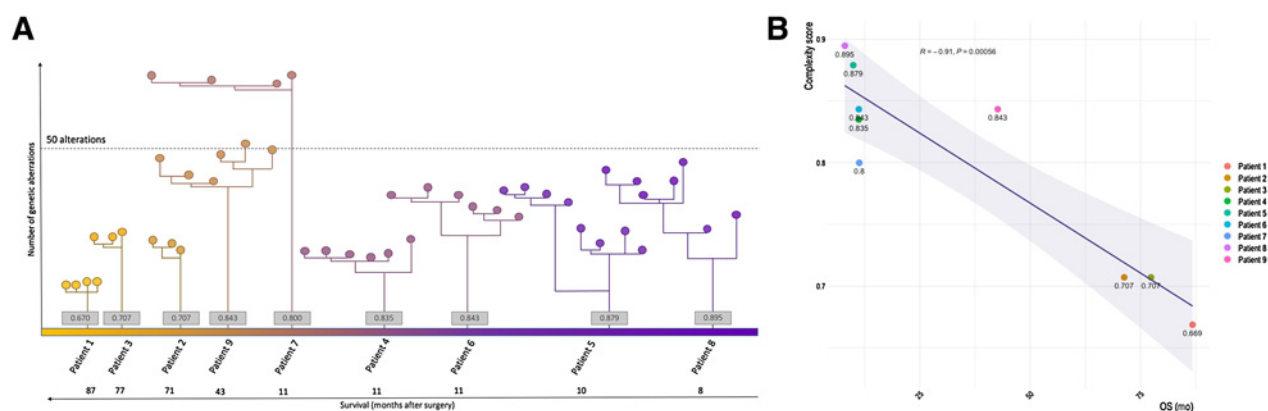


Figure 5. Branching copy-number evolution and patient outcome. **A**, Phylogenetic relationships, made to scale, picturing the genetic clonal landscape of the nine resected pancreatic tumors. The trees are further sorted by overall survival (OS, months), decreasing from left to right. The y-axis corresponds to the absolute number of alterations (CNVs, SNVs, and InDels) detected. The corresponding complexity score for each tree is annotated in gray. **B**, Univariate linear regression comparing phylogenetic tree complexity ($n = 9$) with patient OS (months), whereby an inverse relationship was found ($P < 0.001$).

(referred to as M1-like), CD68⁺CD163⁺ macrophages (referred to as M2-like), CD56⁺CD3⁻ natural killer (NK) cells, CD56⁺CD3⁺ NK cells (referred to as NKT-like cells), and immature CD1a⁺ dendritic cells (referred to as DC_{imm}). In addition, the abundance of CD20⁺ B cells and the total number of B cell aggregates harboring CD8⁺ cells were denoted. PD-L1 expression on both ICs (PD-L1_{IC}) and tumor cells (PD-L1_{TC}) was assessed by single IHC.

To estimate the spatial immunogenic ITH, and its potential association with clonal evolution (complexity score), the median absolute deviation (MAD) from the mean was calculated for all individual immune scores within each tumor. A heterogenous spatial distribution of the ICs, defined as a MAD score > 0, within each primary tumor space was observed for both the abundance and TN infiltration (Fig. 6B). For instance, the abundance of B cells displayed a particularly heterogenous pattern in tumors from patients 1, 3, 6, and 9 (Fig. 6B). However, MAD scores were not calculated for presence of B-cell aggregates or PD-L1_{IC} infiltration due to low overall occurrence (Fig. 6A). Furthermore, no significant associations were found between the degree of spatial distribution of the different IC subsets and phylogenetic complexity (Supplementary File S7, Supplementary Fig. S4). Of note, the surrounding microenvironment in the tumor of patient 9 was characterized by a particularly active immune response (Fig. 6A), dominated by T_C and T_H cells, B cells, PD-L1_{ICs} and M2-like macrophages.

Local immune pressure

Associations between the abundance and infiltration of IC subsets with phylogenetic characteristics and OS were also examined by univariate regression analysis, as shown in Supplementary File S8. A joint value for the abundance and TN infiltration, respectively, of each IC subtype was used to account for interpatient differences in the number of tumor areas analyzed. For PD-L1_{TCs} and ICs with an overall low presence, that is, NK cells, NKT-like cells, DC_{imm}, PD-L1_{ICs}, and B-cell aggregates, and for all TN infiltration scores, the percentage of positively stained cores divided by all cores (% positive/all) was used. The median value was used for all other IC subsets.

The limited number of cases did not allow for adjusted analyses but enabled identification of hypothesis-generating patterns and some noticeable findings. To name some, non-significant trends were seen

toward an association between the abundance of B cells and NK cells and longer OS, and between PD-L1_{TC} expression and shorter OS. Similar trends could also be seen between M2-like macrophage TN infiltration and increased tree complexity, increased treetop length and a shorter OS. The most notable finding was a significant association ($P = 0.005$) between PD-L1_{TC} expression and the treetop length of the phylogeny (Fig. 7A). The distribution of PD-L1_{TC} expression throughout the tumor areas in each SPTC is further visualized in Fig. 7B, together with representative IHC images (Fig. 7C and D).

Discussion

In this study, we provide a detailed description of the geographical genetic clonal evolution through the regional tumor space of nine patients with resected PDAC, also in relation to the immunogenic ITH, with particular emphasis on detecting any potential associations of these features with survival. Recent evolutionary analyses of PDAC have shown that the ITH of driver events is remarkably limited between subclones found in the primary tumor and those detected in metastatic lesions (16, 17). It has, therefore, been argued that PDAC tumor plasticity, and adaption to selection pressures, is mainly a consequence of epigenomic change (33). In line with these findings, variants detected in driver genes throughout this study were primarily observed early on during tumor development, situated in the trunks of the nine evolutionary trees. However, it is important to emphasize that novel driver variants, not included in the targeted sequencing panel and thus not detectable, might still be present in the tree branches. It should also be acknowledged that the produced phylogenies are to be considered estimations of the most probable order in which specific genetic events occur, not approximations of time.

In contrast, genetic ITH was found to varying degrees in all patients when evaluating disparities in CNV profiles throughout the regional tumor areas. These CNVs laid the foundation for the observed phylogenetic branching structure, the complexity of which was found to be associated with survival time. CNVs, including both quantity measures and specific aberrations, have earlier been shown to carry prognostic value in PDAC (12, 34, 35), but this study is, to our knowledge, the first to describe the spatial heterogeneity and evolutionary significance of CNVs in treatment naïve primary PDAC.

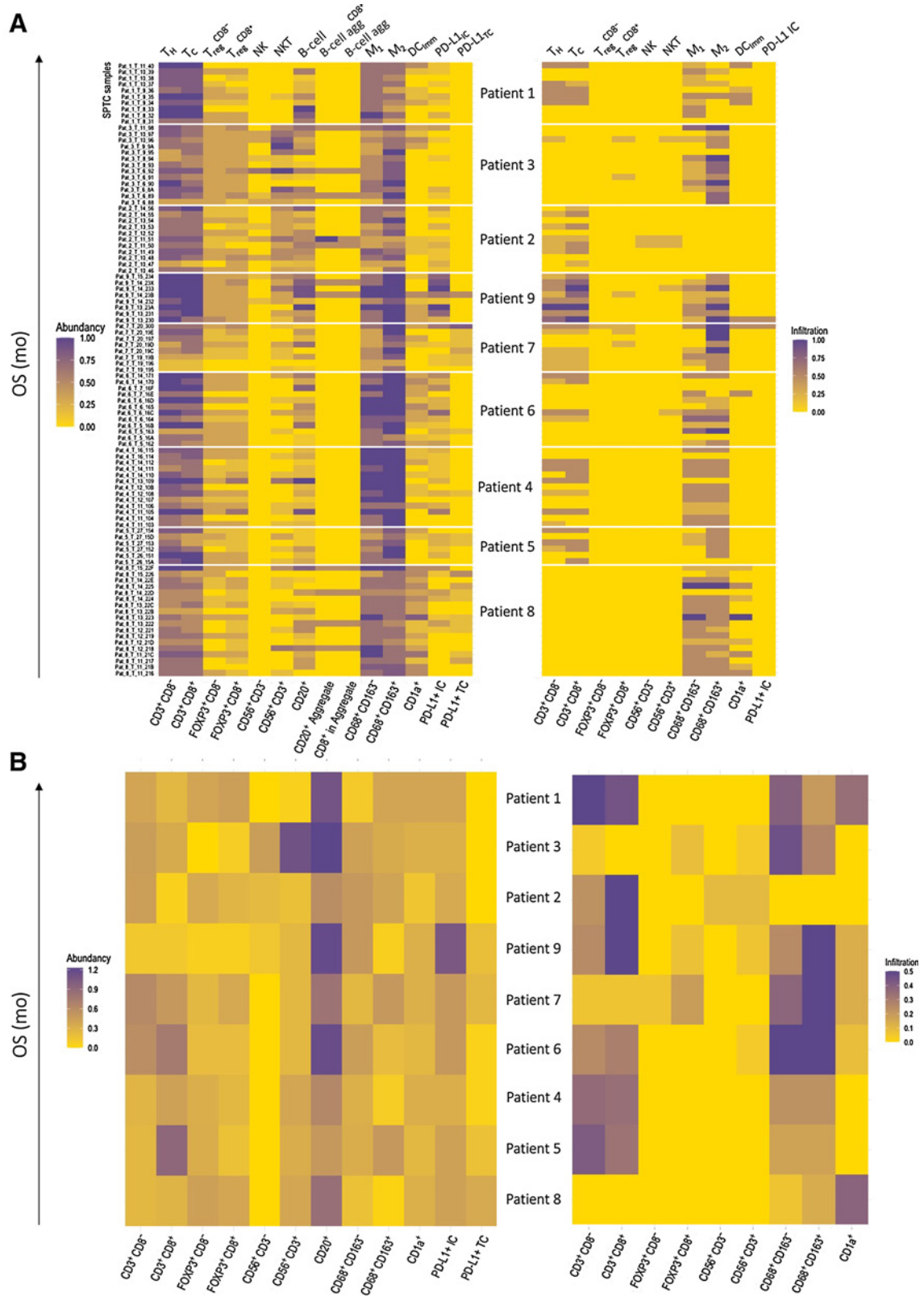


Figure 6. Immune cell abundance and TN infiltration. **A**, Heatmaps illustrating the results following IHC staining of single patient tissue chips (SPTC) constructed for each patient. Abundance (left) and tumor nest (TN) infiltration (right) of the evaluated IC subsets (top), and their corresponding immune markers (bottom) are shown, on a normalized scale from 0 to 1, for all primary tumor areas. The patients are sorted by overall survival (OS, months), decreasing from top to bottom. **B**, Heatmaps visualizing the spatial heterogeneity of each IC subset, both in abundance (left) and TN infiltration (right), again sorted by patient OS. Heterogeneity scores are based on the median absolute deviation from the mean within each tumor, derived from the variations shown in **A**.

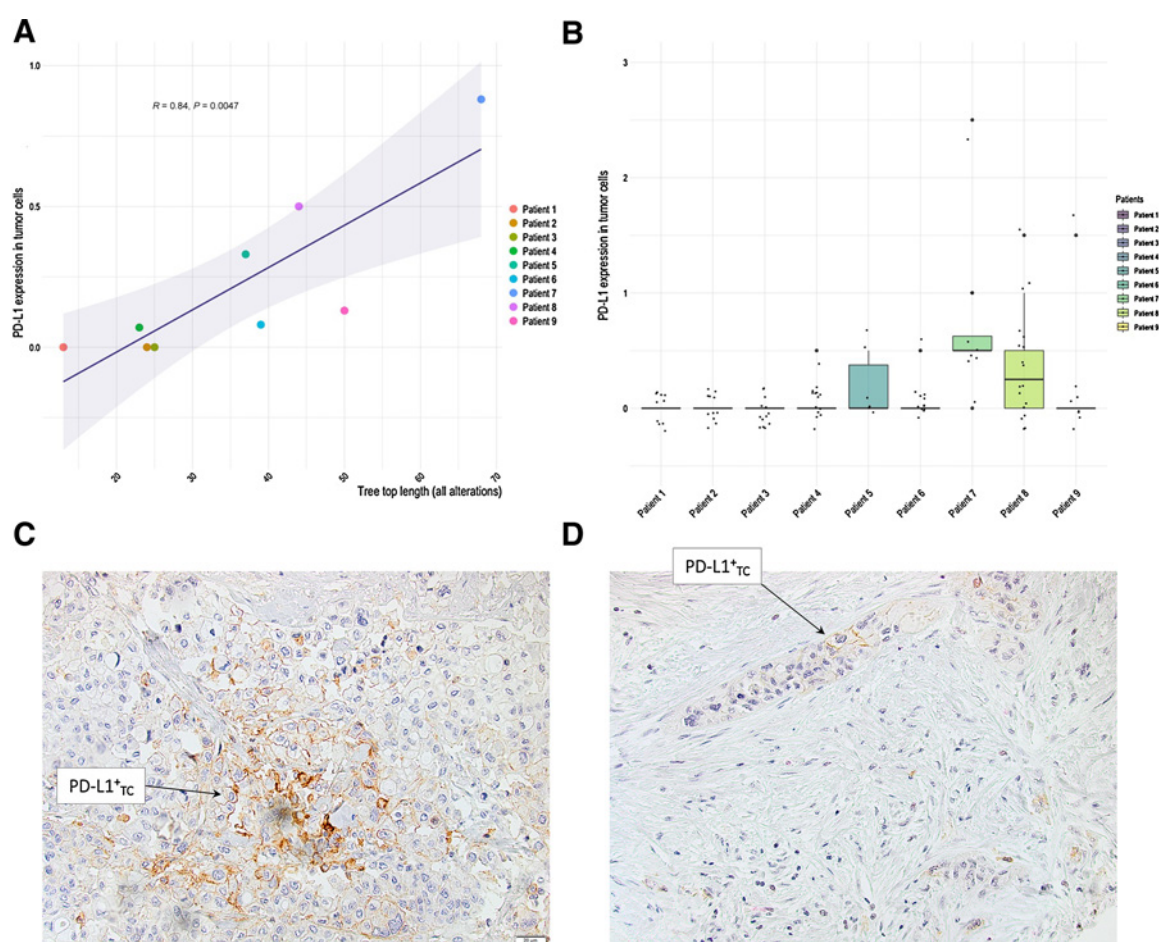


Figure 7. PD-L1 expression on tumor cells and associations with phylogenetic tree top length. **A**, Univariate linear regression comparing a summarizing value of PD-L1 expression in each tumor (PD-L1_{TC}) with the tree top length of each phylogeny ($n = 9$). A significant association ($P = 0.005$) was found between a larger tree and expression of PD-L1_{TC}. **B**, Boxplot showing the distribution of PD-L1_{TC} expression for the different tumor areas in each patient. **C**, Representative IHC image of high (3, range 0–3) PD-L1_{TC} expression and **(D)** intermediate (2, range 0–3) PD-L1_{TC} expression.

However, as the majority of hitherto produced phylogenetic trees in PDAC has been based on SNVs, a second phylogenetic analysis was performed, using all detected point mutations. This additional evaluation did, nevertheless, also show an overall limited ITH of SNVs in the resected tumors. Yet, as TDS is limited to investigating mutations in specific loci, this may have contributed to the restricted observed SNV heterogeneity (17). Still, these results strengthen our hypothesis that integration of CNVs into phylogenetic analyses, following careful definition of chromosomal break points, may increase the ability to unravel possible evolutionary trajectories (28). Our findings are also in agreement with studies on other types of cancer, for instance clear cell renal cell carcinoma, lung cancer, and pediatric solid tumors, where intratumor copy-number heterogeneity has been shown to be of importance for patient survival (27, 36, 37). The outcome of these analyses further stresses the importance of CNVs, such as amplifications or homozygous allelic losses, in tumorigenesis, as the resulting gene alterations may be just as detrimental as mutational variants.

In this study, the visual phylogenetic branching structure was translated into a numerical measure to enable analyses of its relationship to survival time after resection. A network-based complexity score was developed, scalable depending on the number of subclones and

designed to increase with the number of branching generations. A limiting factor of this method is that it only considers the network architecture and not the number of aberrations present, and, hence, not the absolute length of the branches. Therefore, we also examined other more elementary tree attributes, such as the treetop and stem length, in relation to patient outcome. The findings showed that evolutionary complexity was the strongest factor associated with survival time after surgery, in line with recent work on surgically resected mesothelioma (38). Thus, in spite of the small sample size, these results propose that the intratumor copy-number complexity in the regional tumor space of resected PDAC may reflect the evolvability of the tumor before exposure to selection pressures from systemic therapy. It must, however, be pointed out that the definition of a subclone throughout this study is not to be assumed as being causal to a specific tumor cell phenotype, but rather as a way to cluster genetically similar tumor clones.

With regard to potential positive selection of specific CNV events, a recent pan-cancer study has emphasized the evolutionary importance of CNV acquisitions, considering both selection and genetic drift (39). Although no significant associations were detected in the limited case-series in this study, the detailed analysis of common copy-number

changes in PDAC (32) showed that loss of *8p* was exclusively detected in patients with shorter survival. Loss of *8p* has not previously been linked to clinical outcome in PDAC, but has been shown to promote tumor progression in breast cancer (40). However, we did not acknowledge evidence for any copy-number changes to be recurrently appearing solely in the branches of the trees; loss of *8p* was detected in the tree stem in 3 out of 5 cases. As no pronounced evidence for positive selection of neither mutational drivers nor copy-number events was detected, our main hypothesis leans toward the observed branching being a result of neutral evolution, which is also in line with the findings of a limited number of subclonal drivers. An increased clonal complexity, in other words the acquisition of a broad tumor clone repertoire, would thus increase the risk of chemoresistance.

Of note, the high stromal density in pancreatic tumors contributes to a low neoplastic cellularity, thus posing difficulties for studying tumor cell DNA alterations. Consequently, samples containing a high quantity of non-neoplastic cells were excluded from the clonal deconvolution and phylogenetic analysis to avoid underestimation of the genetic subclonal heterogeneity. Statistical analyses indeed confirmed that there were no significant associations between TCF and either tumor complexity or intrapatient subclonal diversity. Furthermore, another possible confounder in need of attention was the number of tumor samples constituting each phylogeny and differences in their geographical distribution. Complexity values were, therefore, also examined in relation to the count of tumor samples included and the number of individual paraffin blocks used, but no sampling bias was detected. Taken together, these findings support the feasibility of using available FFPE tissue for purposes of phylogenetic modeling.

Clonal tumor evolution has further been shown to be in dynamic interplay with the surrounding immune microenvironment, adapting to evade recognition by infiltrating ICs (20, 38). Although pancreatic tumors, with their highly desmoplastic and dense stroma, have been described previously as being comparatively “immunologically cold” (21), several studies have demonstrated that both the type and spatial distribution of infiltrating ICs carry prognostic value in PDAC (22, 41, 42). Throughout the primary tumor regions in the herein examined cases, there was a varying degree of intrapatient as well as interpatient heterogeneity regarding both the abundance and TN infiltration of different IC subsets. We hypothesized that spatial genetic heterogeneity would also be reflected in alterations of the corresponding surrounding immune microenvironment, in relation to both the quantity of DNA alterations and specific subclonal mutations. We were, however, not able to detect any significant associations between a complex phylogeny and heterogenous patterns of either the abundance or TN infiltration for any of the investigated IC subsets. Additional studies on larger patient series are, therefore, needed to shed further light on the question of how and to what extent the immune microenvironment might influence clonal evolution in PDAC. A relevant starting point could be to evaluate links between specific genetic immune evasion traits of the tumor cells, neoantigen repertoire, and the immune phenotype of each tumor region, as this has been shown to be important in other tumor types (20, 38).

Although the limited number of cases included in this study did not allow for any strong conclusions to be drawn regarding the prognostic value of different IC subsets, their spatial diversity is clearly demonstrated, which further emphasizes the importance of considering more than one tumor area in biomarker studies (43). In addition, some non-significant trends toward prognostic associations that are congruent with previous findings were indeed detected in our small cohort, such as between an increased abundance of NK cells and B cells and a

prolonged survival (41, 42), or an increased infiltration of M2 polarized macrophages and a shorter OS (44).

A noteworthy finding is the highly active immune microenvironment observed throughout all tumor regions of patient 9. Genomic profiling of this tumor revealed a copy-number amplification of segment 9p.22 in the phylogenetic tree trunk, covering the *FREMI* gene, which has recently been linked to increased IC infiltration and an improved outcome in breast cancer (45, 46). These findings, along with the complex evolutionary trajectory and the comparatively long postsurgical survival time (43 months) of this patient, could suggest that, under certain circumstances, an active immune response might balance the negative prognostic impact of an evolutionary prone tumor. In this context, *FREMI* alterations merit further study, not only as a biomarker of an active local immune response, but also in terms of molecular targeted and/or immune checkpoint inhibiting treatment approaches.

Immune modulatory therapies have been evaluated as a treatment option for PDAC, but very little effectiveness has been reported so far (47). Thus, beyond analyses of distinct IC subsets, we also set out to investigate if expression of the inhibitory ligand PD-L1, on both leukocytes and tumor cells, might be linked to tumor evolution. Of note, a significant positive association was found between PD-L1 expression on tumor cells and the length of the phylogenetic tree. Speculatively, this may suggest that an increase in CNVs demands suppression of the immune system to evade recognition. In line with this hypothesis, a previous study demonstrated a correlation between the dosage of CNVs and markers of immune evasion (48).

The only potentially curative treatment for patients diagnosed with PDAC includes surgical removal of the tumor followed by an maximum tolerated dose (MTD) of cytotoxic chemotherapy, with the aim to eradicate any residual microscopic disease. However, treatment resistance remains a major threat as most patients die of recurrent disease, and the risk of suffering from negative side effects and a decreased quality of life often surpasses the survival benefit from chemotherapy. In this regard, the herein performed comprehensive analyses have culminated in novel insights into the genetic evolvability of treatment naïve primary resected PDAC. In particular, the potential association between branching copy-number evolution and survival merits further study. If validated in a larger cohort, including patients with non-resectable tumors, these findings could also for instance encourage the use of evolutionary strategies for systemic treatment of PDAC, as has previously shown to be effective in metastatic prostate cancer (49). Along this line, it could be hypothesized that patients with a homogenous genetic profile throughout their primary tumor, signifying a lower ability of the tumor to evolve and adapt, will have a more indolent disease and, hence, benefit from linear adjuvant treatment according to current protocols. On the other hand, in patients with tumors displaying complex evolutionary patterns, suggesting an increased evolvability, chemotherapy administered at the MTD might instead accelerate the selection of treatment-resistant clones (2). These patients might, therefore, instead benefit from surveillance with on-treatment liquid biopsies and treatment strategies where the dosage is adjusted according to quantitative tumor responses, or where multiple therapies are applied sequentially according to qualitative tumor alterations.

To conclude, this study sheds further light on the copy-number evolution of resectable primary PDAC. The results indicate that multiregional genetic profiling of the primary tumor and available lymph node metastases, followed by phylogenetic analysis, may provide important information on the evolutionary propensity of treatment naïve pancreatic tumors. In addition, a few

hypothesis-generating findings in relation to the surrounding immune microenvironment were detected, suggesting that its potential influence on clonal evolution in PDAC remains a topic of interest for further study.

Authors' Disclosures

K. Leandersson reports personal fees from Cantargia AB outside the submitted work. No disclosures were reported by the other authors.

Disclaimer

None of the funding bodies had any role in the design of the study and collection, analysis, and interpretation of data or in writing the article.

Authors' Contributions

A. Petersson: Conceptualization, data curation, formal analysis, investigation, visualization, methodology, writing—original draft, project administration, writing—review and editing. **N. Andersson:** Software, formal analysis, visualization, methodology, writing—review and editing. **S.O. Hau:** Resources, formal analysis, writing—review and editing. **J. Eberhard:** Resources, supervision, writing—review and editing. **J. Karlsson:** Methodology, writing—review and editing. **S. Chattopadhyay:** Data curation, formal analysis, investigation, methodology, writing—review and editing. **A. Valind:** Data curation, formal analysis, methodology, writing—review and editing. **J. Elebro:** Resources, data curation, writing—review and editing. **B. Nodin:** Resources,

methodology, writing—review and editing. **K. Leandersson:** Conceptualization, data curation, supervision, writing—review and editing. **D. Gisselsson:** Conceptualization, data curation, supervision, funding acquisition, methodology, writing—review and editing. **K. Jirström:** Conceptualization, resources, data curation, formal analysis, supervision, funding acquisition, investigation, methodology, writing—original draft, project administration, writing—review and editing.

Acknowledgments

This study was supported by grants from the Swedish Research Council (grant numbers 2015-03598 and 2018-02441; to K. Jirström), the Swedish Cancer Society (grant numbers CAN 2016/483 and CAN 2018/418; to K. Jirström), the Sjöberg Foundation (to K. Jirström, K. Leandersson, and D. Gisselsson), the Lennart Glans Foundation, BioCARE, the Berta Kamprad Foundation (to K. Jirström), the Governmental Funding of Clinical Research within the National Health Service (ALF; to K. Jirström), Skåne University Hospital Funds and Donations (to K. Jirström), and the Faculty of Medicine, Lund University (to K. Jirström).

The costs of publication of this article were defrayed in part by the payment of page charges. This article must therefore be hereby marked *advertisement* in accordance with 18 U.S.C. Section 1734 solely to indicate this fact.

Received November 23, 2021; revised January 5, 2022; accepted February 4, 2022; published first February 11, 2022.

References

- Greaves M. Darwinian medicine: a case for cancer. *Nat Rev Cancer* 2007;7:213–21.
- Gillies RJ, Verduzco D, Gatenby RA. Evolutionary dynamics of carcinogenesis and why targeted therapy does not work. *Nat Rev Cancer* 2012;12:487–93.
- Welch DR. Tumor heterogeneity—a 'contemporary concept' founded on historical insights and predictions. *Cancer Res* 2016;76:4–6.
- Ferlay J, Colombet M, Soerjomataram I, Dyba T, Randi G, Bettio M, et al. Cancer incidence and mortality patterns in Europe: estimates for 40 countries and 25 major cancers in 2018. *Eur J Cancer* 2018;103:356–87.
- Ferlay J, Soerjomataram I, Dikshit R, Eser S, Mathers C, Rebelo M, et al. Cancer incidence and mortality worldwide: sources, methods and major patterns in GLOBOCAN 2012. *Int J Cancer* 2015;136:E359–86.
- Siegel RL, Miller KD, Jemal A. Cancer statistics, 2020. *CA Cancer J Clin* 2020;70:7–30.
- Carioli G, Malvezzi M, Bertuccio P, Boffetta P, Levi F., La Vecchia C, et al. European cancer mortality predictions for the year 2021 with focus on pancreatic and female lung cancer. *Ann Oncol* 2021;32:478–87.
- GBD 2017 Pancreatic Cancer Collaborators. The global, regional, and national burden of pancreatic cancer and its attributable risk factors in 195 countries and territories, 1990–2017: a systematic analysis for the global burden of disease study 2017. *Lancet Gastroenterol Hepatol* 2019;4:934–47.
- Vincent A, Herman J, Schulick R, Hruban RH, Goggins M. Pancreatic cancer. *Lancet* 2011;378:607–20.
- Groot VP, Rezaee N, Wu W, Cameron JL, Fishman EK, Hruban RH, et al. Patterns, timing, and predictors of recurrence following pancreatotomy for pancreatic ductal adenocarcinoma. *Ann Surg* 2018;267:936–45.
- Bailey P, Chang DK, Nones K, Johns AL, Patch AM, Gingras MC, et al. Genomic analyses identify molecular subtypes of pancreatic cancer. *Nature* 2016;531:47–52.
- Waddell N, Pajic M, Patch AM, Chang DK, Kassahn KS, Bailey P, et al. Whole genomes redefine the mutational landscape of pancreatic cancer. *Nature* 2015;518:495–501.
- Bailey MH, Meyerson WU, Dursi LJ, Wang LB, Dong G, Liang WW, et al. Retrospective evaluation of whole exome and genome mutation calls in 746 cancer samples. *Nat Commun* 2020;11:4748.
- Campbell PJ, Yachida S, Mudie LJ, Stephens PJ, Pleasance ED, Stebbings LA, et al. The patterns and dynamics of genomic instability in metastatic pancreatic cancer. *Nature* 2010;467:1109–13.
- Jones S, Zhang X, Parsons DW, Lin JC, Leary RJ, Angenendt P, et al. Core signaling pathways in human pancreatic cancers revealed by global genomic analyses. *Science* 2008;321:1801–6.
- Yachida S, Jones S, Bozic I, Antal T, Leary R, Fu B, et al. Distant metastasis occurs late during the genetic evolution of pancreatic cancer. *Nature* 2010;467:1114–7.
- Makohon-Moore AP, Zhang M, Reiter JG, Bozic I, Allen B, Kundu D, et al. Limited heterogeneity of known driver gene mutations among the metastases of individual patients with pancreatic cancer. *Nat Genet* 2017;49:358–66.
- Sakamoto H, Attiyeh MA, Gerold JM, Makohon-Moore AP, Hayashi A, Hong J, et al. The evolutionary origins of recurrent pancreatic cancer. *Cancer Discov* 2020;10:792–805.
- Notta F, Chan-Seng-Yue M, Lemire M, Li Y, Wilson GW, Connor AA, et al. A renewed model of pancreatic cancer evolution based on genomic rearrangement patterns. *Nature* 2016;538:378–82.
- Rosenthal R, Cadieux EL, Salgado R, Bakir MA, Moore DA, Hiley CT, et al. Neoantigen-directed immune escape in lung cancer evolution. *Nature* 2019;567:479–85.
- Knudsen ES, Vail P, Balaji U, Ngo H, Botros IW, Makarov V, et al. Stratification of pancreatic ductal adenocarcinoma: combinatorial genetic, stromal, and immunologic markers. *Clin Cancer Res* 2017;23:4429–40.
- Wartenberg M, Cibin S, Zlobec I, Vassella E, Eppenberger-Castori S, Terracciano L, et al. Integrated genomic and immunophenotypic classification of pancreatic cancer reveals three distinct subtypes with prognostic/predictive significance. *Clin Cancer Res* 2018;24:4444–54.
- Hau SO, Petersson A, Nodin B, Karnevi E, Boman K, Williamsson C, et al. Chemotherapy, host response and molecular dynamics in periampullary cancer: the CHAMP study. *BMC Cancer* 2020;20:308.
- Rasmussen M, Sundstrom M, Goransson Kultima H, Botling J, Micke P, Birgisson H, et al. Allele-specific copy number analysis of tumor samples with aneuploidy and tumor heterogeneity. *Genome Biol* 2011;12:R108.
- Staaf J, Lindgren D, Vallon-Christersson J, Isaksson A, Goransson H, Juliusson G, et al. Segmentation-based detection of allelic imbalance and loss-of-heterozygosity in cancer cells using whole genome SNP arrays. *Genome Biol* 2008;9:R136.
- Mengelbier LH, Karlsson J, Lindgren D, Valind A, Lilljebjorn H, Jansson C, et al. Intratumoral genome diversity parallels progression and predicts outcome in pediatric cancer. *Nat Commun* 2015;6:6125.
- Andersson N, Bakker B, Karlsson J, Valind A, Holmquist Mengelbier L, Spierings DCJ, et al. Extensive clonal branching shapes the evolutionary history of high-risk pediatric cancers. *Cancer Res* 2020;80:1512–23.
- Andersson N, Chattopadhyay S, Valind A, Karlsson J, Gisselsson D. DEVOLUTION-A method for phylogenetic reconstruction of aneuploid cancers based on multiregional genotyping data. *Commun Biol* 2021;4:1103.

29. Martin JK, Hirschberg D. On the complexity of learning decision trees. *International Symposium on Artificial Intelligence and Mathematics* 1996. p. 112–5.
30. Wickham H. *ggplot2: Elegant Graphics for Data Analysis*. New York: Springer-Verlag; 2016.
31. R Core Team. *R: a language and environment for statistical computing*. Vienna, Austria: R Foundation for Statistical Computing; 2019. Available from: <https://www.R-project.org/>.
32. Sandhu V, Wedge DC, Bowitz Lothe IM, Labori KJ, Dentre SC, Buanes T, et al. The genomic landscape of pancreatic and periampullary adenocarcinoma. *Cancer Res* 2016;76:5092–102.
33. McDonald OG, Li X, Saunders T, Tryggvadottir R, Mentch SJ, Warmoes MO, et al. Epigenomic reprogramming during pancreatic cancer progression links anabolic glucose metabolism to distant metastasis. *Nat Genet* 2017;49:367–76.
34. Asting AG, Ljungman D, Caren H, Dambrauskas Z, Iresjo BM, Hyltander A, et al. Alterations in tumor DNA are related to short postoperative survival in patients resected for pancreatic carcinoma aimed at cure. *Pancreas* 2016;45: 900–7.
35. Donahue TR, Tran LM, Hill R, Li Y, Kovochich A, Calvopina JH, et al. Integrative survival-based molecular profiling of human pancreatic cancer. *Clin Cancer Res* 2012;18:1352–63.
36. Turajlic S, Xu H, Litchfield K, Rowan A, Horswell S, Chambers T, et al. Deterministic evolutionary trajectories influence primary tumor growth: TRACERx renal. *Cell* 2018;173:595–610.
37. Jamal-Hanjani M, Wilson GA, McGranahan N, Birkbak NJ, Watkins TBK, Veeriah S, et al. Tracking the evolution of non-small cell lung cancer. *N Engl J Med* 2017;376:2109–21.
38. Zhang M, Luo JL, Sun Q, Harber J, Dawson AG, Nakas A, et al. Clonal architecture in mesothelioma is prognostic and shapes the tumour microenvironment. *Nat Commun* 2021;12:1751.
39. Watkins TBK, Lim EL, Petkovic M, Elizalde S, Birkbak NJ, Wilson GA, et al. Pervasive chromosomal instability and karyotype order in tumour evolution. *Nature* 2020;587:126–32.
40. Cai Y, Crowther J, Pastor T, Abbasi Asbagh L, Baietti MF, De Troyer M, et al. Loss of chromosome 8p governs tumor progression and drug response by altering lipid metabolism. *Cancer Cell* 2016;29:751–66.
41. Lundgren S, Elebro J, Heby M, Nodin B, Leandersson K, Micke P, et al. Quantitative, qualitative and spatial analysis of lymphocyte infiltration in periampullary and pancreatic adenocarcinoma. *Int J Cancer* 2020;146: 3461–73.
42. Lundgren S, Micke P, Elebro J, Heby M, Hrynchyk I, Nodin B, et al. Topographical distribution and spatial interactions of innate and semi-innate immune cells in pancreatic and other periampullary adenocarcinoma. *Front Immunol* 2020;11:558169.
43. Gerlinger M, Rowan AJ, Horswell S, Math M, Larkin J, Endesfelder D, et al. Intratumor heterogeneity and branched evolution revealed by multiregion sequencing. *N Engl J Med* 2012;366:883–92.
44. Hu H, Hang JJ, Han T, Zhuo M, Jiao F, Wang LW. The M2 phenotype of tumor-associated macrophages in the stroma confers a poor prognosis in pancreatic cancer. *Tumour Biol* 2016;37:8657–64.
45. Li HN, Li XR, Lv ZT, Cai MM, Wang G, Yang ZF. Elevated expression of FREM1 in breast cancer indicates favorable prognosis and high-level immune infiltration status. *Cancer Med* 2020;9:9554–70.
46. Xu XY, Guo WJ, Pan SH, Zhang Y, Gao FL, Wang JT, et al. TILRR (FREM1 isoform 2) is a prognostic biomarker correlated with immune infiltration in breast cancer. *Aging* 2020;12:19335–51.
47. Taube JM, Klein A, Brahmer JR, Xu H, Pan X, Kim JH, et al. Association of PD-1, PD-1 ligands, and other features of the tumor immune microenvironment with response to anti-PD-1 therapy. *Clin Cancer Res* 2014;20:5064–74.
48. Davoli T, Uno H, Wooten EC, Elledge SJ. Tumor aneuploidy correlates with markers of immune evasion and with reduced response to immunotherapy. *Science* 2017;355:eaaf8399.
49. Zhang J, Cunningham JJ, Brown JS, Gatenby RA. Integrating evolutionary dynamics into treatment of metastatic castrate-resistant prostate cancer. *Nat Commun* 2017;8:1816.